Published in final edited form as:
Cerebellum. 2012 March ; 11(1): 121–131. doi:10.1007/s12311-009-0151-3.

Calcium Influx Measured at Single Presynaptic Boutons of Cerebellar Granule Cell Ascending Axons and Parallel Fibers

Wei Zhang and **David J. Linden**
Department of Neuroscience, The Johns Hopkins University, 725 North Wolfe St, Baltimore, MD 21205, USA

David J. Linden: dlinden@jhmi.edu

Abstract

Action potential-evoked calcium influx into presynaptic boutons is a key determinant of synaptic strength and function. Here, we have examined the calcium dynamics at individual presynaptic boutons of the cerebellar granule cells in the molecular layer of cerebellar slices and investigated whether different subpopulations of granule cell boutons exhibit different calcium dynamics. We found that a population of boutons with low basal calcium clearance rates may activate a second clearance mechanism and exhibit biphasic calcium decay on high calcium influx induced by bursts of action potentials. We also found that boutons on ascending axons and parallel fibers show similar calcium influx amplitudes and calcium clearance rates in response to action potentials. Lastly, we found that parallel fiber boutons located in the inner molecular layer have a higher calcium clearance rate than boutons located in the outer molecular layer. These results suggest that cerebellar granule cell boutons should not be regarded as a homogeneous population, but rather that different subpopulations of boutons may exhibit different properties. The heterogeneity of presynaptic boutons may allow different learned behaviors to be encoded in the same circuit without mutual interference and may be a general mechanism for increasing the computational capacity of the brain.

Keywords

Presynaptic bouton; Calcium imaging; Parallel fiber; Ascending axon; Cerebellar granule cell

Introduction

The cerebellum plays an important role in the integration of sensory information and its transformation into coordinated motor output. To perform this function, the cerebellum receives two major excitatory inputs, climbing fibers and mossy fibers. Mossy fibers form synapses on granule cells in the granule cell layer of the cerebellum, which in turn send ascending axons (AAs) into the molecular layer, where they bifurcate into parallel fibers (PFs) which extend for several millimeters in the transverse plane, orthogonal to the plane of the Purkinje cell (PC) dendrites [1,2]. Both AAs and PFs form functional synapses with PCs. This circuit diagram has led to the development of the “beam hypothesis” as a dominant model of cerebellar function [3,4]. The beam hypothesis posits that focal activation of the granule cell layer will activate a beam of PCs up and down the folium, with lateral inhibition by basket and stellate cells suppressing PC activity in adjacent beams. This hypothesis is

Correspondence to: David J. Linden, dlinden@jhmi.edu.

Electronic supplementary material The online version of this article (doi:10.1007/s12311-009-0151-3) contains supplementary material, which is available to authorized users.

supported by early electrophysiological recording studies in which PFs were stimulated directly [5], as well as some more recent optical imaging measurements [6]. However, other studies utilizing in vivo recording with natural tactile stimuli [7-9] and optical imaging of the whole cerebellum [10,11] have shown that mossy fiber activation of granule cells generally results in activation of patches of PCs. These studies have in turn led to an alternative "patch hypothesis" of cerebellar function, which posits that the cerebellum is organized functionally into vertical columns. Two major mechanisms have been proposed to explain how the circuitry of the cerebellum can give rise to a patchy activation of PCs [12]. Firstly, lateral and feedforward inhibition by interneurons in the molecular layer can serve to shape PF inputs to PCs such that only a patch of PCs are activated. [11]. Secondly, it has been proposed that granule cell activation of PCs can be divided into two forms, a strong activation occurring through AA-PC synapses, and a weaker modulatory activation occurring through PF-PC synapses ([9,13,14], but see [15,16]).

The proposal that AA-PC synapses are stronger than PF-PC synapses is supported by several anatomical differences. Firstly, AAs form multiple synapses primarily with a single PC en route to the molecular layer, while each PC receives only one to two synapses with any single PF. Nevertheless, due to the greater length of the PFs compared to the AAs, PF-PC synapses constitute 80–97% of the total number of granule cell axon-PC synapses [17]. Secondly, presynaptic boutons on AAs are larger in size than that on PFs, suggesting a more powerful synaptic connection [2]. Thirdly, AAs and PFs synapse on different dendritic compartments on PCs, with AAs forming synapses on small-diameter PC dendrites and PFs forming synapses on both large- and small-diameter PC dendrites [18,19].

A functional division between AA and PF synapses is also supported by in vitro studies showing functional differences between the two classes of synapses. Electrophysiological recordings in acute cerebellar slices have suggested that AA synapses release neurotransmitter with higher mean release probability and quantal amplitude [13] and are more resistant to long-term depression and potentiation [14] compared to PF synapses. However, other studies have suggested that AA and PF synapses are functionally similar. Specifically, studies examining unitary granule cell-PC synapses using electrical stimulation [15] and photostimulation [16] have found AA-PC and PF-PC synapses to be indistinguishable in strength. Therefore, despite the wealth of data available on the properties of AAs versus PFs, there is still considerable uncertainty regarding their functional equivalence, and additional detailed studies of individual boutons on AAs and PFs may shed more light on the subject.

In addition to the possible functional difference between AAs and PFs, PFs in different regions of the molecular layer may also be functionally different. PFs in the molecular layer are arranged in a highly topographical manner, with granule cells in the inner granule cell layer giving rise to PFs in the inner molecular layer and granule cells in the outer granule cell layer giving rise to PFs in the outer molecular layer. Previous studies suggest that cells located in different granule cell layers may receive inputs from different regions of the brain. Specifically, it has been suggested that spinocerebellar and pontocerebellar fibers may form synapses with deep and superficial granule cells respectively [4], although other studies have found no evidence of layer-specific termination for mossy fibers from difference sources [2]. Aside from possible differences in inputs, PFs in the inner and outer molecular layers also differ in other anatomical parameters. Compared to PFs in the outer molecular layer, PFs in the inner molecular layer are shorter in length and thicker in diameter near the bifurcation branch point [17,20], with fiber diameter decreasing with distance from the branch point. PFs in the inner molecular layer also have larger boutons which tend to be clustered near the branch point and contain multiple active zones [17]. By contrast, PFs in the outer molecular layer are longer and uniformly thin and possess smaller boutons. Based on these anatomical

differences, it has been suggested that granule cell axons bifurcating in the inner molecular layer possess shorter AAs and, hence, activate PCs mainly through the large PF boutons clustered near the branch points, whereas axons bifurcating in the outer molecular layer possess longer AAs and may activate PCs mainly through their AA boutons, with the PF boutons having a modulatory role [17]. Another source of possible functional specialization between inner and outer molecular layer PFs may be the difference in their postsynaptic targets. PFs in the inner molecular layer innervate proximal regions of PC dendrites, where their synapses are expected to be intercalated with climbing fiber-PC synapses, as well as basket cell interneurons located exclusively in the inner molecular layer. PFs in the outer molecular layer innervate distal dendritic regions in PCs, which lack climbing fiber innervations and also innervate stellate cell interneurons located in the outer molecular layer. While a variety of factors suggest that PFs in the inner and outer molecular layers may be functionally distinct, to date, no study has directly shown a functional difference between the two types of PFs.

The strength of a synapse is dependent on characteristics of both the presynaptic and the postsynaptic compartments. Postsynaptically, synaptic strength is determined by factors such as neurotransmitter receptor density and unitary conductance. Presynaptically, synaptic strength is dependent on factors such as the size of the readily releasable pool of synaptic vesicles, the neurotransmitter content of each vesicle, as well as the release probability of each vesicle upon the arrival of an action potential. Calcium influx into the presynaptic bouton through voltage-gated calcium channels is a major determinant of release probability. In neurons that fire in bursts, calcium summation and clearance are additional factors that affect neurotransmitter release and synaptic strength. Recent studies have shown that in vivo cerebellar granule cells respond to mossy fiber input by firing in bursts [21-24]. The modulation of calcium dynamics at the granule cell presynaptic bouton may therefore be a major mechanism for the regulation of information flow in the cerebellum. Classical studies of calcium dynamics in presynaptic boutons have examined either specialized giant terminals which can be directly patched and loaded with calcium-binding fluorescent dyes [25] or have utilized bulk loading of acetoxy methylester-derivitized dyes into populations of presynaptic terminals [26]. More recently, a few studies have started to examine calcium dynamics in small individual en passant boutons [27], including studies focusing on the boutons of the cerebellar PFs [28,29]. Here, we utilize a novel sparse loading technique to simultaneously label multiple cerebellar granule cell axons in the molecular layer of cerebellar slices. The increased throughput of this technique has allowed us to measure calcium dynamics at more than a hundred presynaptic boutons of cerebellar granule cells, allowing us to compare the calcium dynamics of boutons located on AAs and PFs, as well as in different regions of the molecular layer.

Materials and Methods

Slice Preparation

Experiments were performed according to guidelines approved by the Animal Care and Use Committee of The Johns Hopkins University School of Medicine. P17-20 Sprague Dawley rats were anesthetized with isoflurane and decapitated, and 250–300-μm thick transverse cerebellar slices were cut by using a vibrating tissue slicer (Leica VT1000S) in ice-cold modified artificial cerebrospinal fluid (ACSF) containing (in millimolar): 120 CholineCl, 2.5 KCl, 1.2 NaH_2PO_4, 25 $NaHCO_3$, 1.0 $CaCl_2$, 7.0 $MgCl_2$, 2.4 Na pyruvate, 1.3 Na ascorbate, and 20 D-glucose. Recovery of slices was performed in a submerged chamber containing oxygenated normal ACSF at 32°C for 30 min. Thereafter, slices were kept at room temperature for the rest of the day until use. Normal ACSF contained (in millimolar): 124 NaCl, 2.5 KCl, 2.5 $CaCl_2$, 1.3 $MgCl_2$, 26.2 $NaHCO_3$, 1 NaH_2PO_4, and 11 D-glucose. Solutions were equilibrated with 95% O_2/5% CO_2 before use.

Dye Loading

After recovery, slices were transferred to a submerged recording chamber where they were continuously perfused with ACSF at a flow rate of 3–4 ml min^{-1}, maintained at 32°C using an in-line heater (Warner Instruments). The granule cell layer was locally perfused with a hypotonic solution containing 1% dextran-conjugated Alexa fluor 594 (10,000 MW; Invitrogen), 10% dextran-conjugated fluo-4 (10,000 MW; Invitrogen), and 15 mM HEPES (modified from [30]). Similar hypotonic loading protocols have also been used in other studies [30,31]. The detailed mechanism of the hypotonic loading method is unknown but may involve hypotonic shock-induced pinocytotic uptake of dye. The dye-loading solution was delivered by positive pressure through a glass pipette with tip size 6–10 μm. To remove excess dye and minimize non-specific loading, a suction pipette with tip size 20–30 μm was placed adjacent to the dye-loading region, at a distance of 200–300 μm above the slice surface. After loading, slices were incubated at 32°C in running normal ACSF for at least 2 h, allowing the dye to diffuse and equilibrate to steady-state levels [30]. Imaging experiments were performed 2–4 h after dye loading.

Single-Photon Confocal Imaging and Data Analysis

Imaging experiments were performed at 32°C both in normal ACSF and in ACSF with fast synaptic transmission blocked. To block fast synaptic transmission, normal ACSF was supplemented with synaptic blockers including 10 μM SR95531 (Ascent Scientific), a $GABA_A$ receptor antagonist; 50 μM D-2-amino-5-phosphonovalerate (D-APV; Ascent Scientific), an N-methyl-D-aspartate (NMDA) receptor antagonist; and 10 μM NBQX-Na_2 (Ascent Scientific), an α-amino-3-hydroxyl-5-methyl-4-isoxazole-propionate (AMPA) receptor antagonist. Imaging was performed using a Zeiss LSM 510 single-photon confocal microscope equipped with a 60×, 0.9 numerical aperture water-immersion objective (LUMPlanFI, Olympus Optical, Tokyo, Japan). Dye-loaded axons were visualized by exciting Alexa fluor 594 with the 543-nm line of the HeNe laser, and the emitted red fluorescence was detected through a 560-nm long-pass filter. Individual boutons were identified as varicosities along the PFs [2,17]. The action potential-evoked Ca^{2+} transient was monitored with the Fluo-4 dye, which was excited using the 488-nm line of an argon laser, and the emitted green fluorescence was detected through a 505-nm long-pass filter. Action potentials were evoked using extracellular stimulation with a glass pipette containing normal ACSF and 0.01% Texas red dextran (Invitrogen), which allowed us to visualize the pipette position under HeNe laser scanning. The stimulating pipette was placed within 20 μm of the dye-loaded target axon and at least 50 μm away from the boutons examined for Ca^{2+} influx. For single stimulation, a test pulse (8–20 μA, 200 μm) was delivered every 30 s; for burst stimulation, a train of four test pulses (10-30 μA, 200 μm) at 100 Hz was delivered every 60 s. Ca^{2+} influx at individual boutons was measured using 1–2% argon laser power under line scan mode at 526 Hz with 1.99 Airy units pinhole size (optical slice thickness less than 3 μm). The scan line was oriented perpendicular to the axon. When multiple boutons on the same axon were compared, line scans were performed on the same bouton repetitively, and responses of different boutons were measured sequentially. At the end of each experiment, the axon morphology was acquired as a Z-stack with 0.5 μm z-axis interval and 512×512 XY frame scans at digital zoom 2 (yielding a pixel size of 0.15 μm) using 60% HeNe laser power with a 0.99 Airy unit pinhole size (optical slice thickness <1.8 μm). Ca^{2+} imaging line scan data were collected and analyzed with Zeiss LSM software. Background correction was first performed by subtracting the background fluorescence of a representative neighboring region next to the bouton. Ca^{2+} signal amplitudes were expressed as $\Delta F/F=(F_t-F_0)/F_0$, with the average fluorescence intensity in the baseline period taken as F_0. The peak Ca^{2+} influx amplitude and the time constant of Ca^{2+} decay were calculated by fitting the data to a single-exponential decay curve using Igor Pro software. The Z-stack data for axon morphology were analyzed using ImageJ (NIH). The images in the Z-stack were

first processed using a median filter with 2 pixel radius to minimize noise and then projected in the z-axis, summing pixel densities for each optical slice. The bouton morphology was manually outlined on the projected image, and relative bouton volume was calculated from the summed integrated density of the bouton. For a given concentration of fluorescent dye, integrated density is directly proportional to relative volume. To estimate the concentration of dye within boutons, the mean pixel intensity of Alexa 594 of each bouton in the Z-stack was also determined. Group data of all imaging experiments are reported as mean ± SEM unless otherwise specified and compared statistically using paired Student's *t* test. A significance of $p<0.05$ is indicated by an asterisk, and a significance of $p<0.01$ is indicated by two asterisks.

Results

Cerebellar granule cells were loaded with the calcium-sensitive dye dextran-conjugated fluo-4 and the morphology dye dextran-conjugated Alexa fluor 594 by local perfusion of the dyes in a detergent-free solution at the cerebellar granule cell layer. After a 2-h recovery period for dye diffusion and equilibration, presynaptic boutons are clearly visualized as bead-like swellings along AAs and PFs in the cerebellar molecular layer (Fig. 1a; see also [29]). Data from both AA and PF boutons were pooled, with 12 AA boutons and 103 PF boutons in the dataset. To measure calcium dynamics at individual boutons, line scans were performed across individual boutons, and fluorescence from the calcium-sensitive dye was measured. Calcium transients in the presynaptic boutons were evoked with a stimulating electrode placed in the granule cell layer, and the stimulus consisted of a single pulse followed 500 ms later by a burst of four pulses at 100 Hz. This stimulation reliably evoked action potentials, which propagated into presynaptic boutons without failure, and induced a single action potential-evoked calcium transient followed by a larger burst calcium transient caused by the summation of four consecutive calcium transients (Fig. 1b). At each individual bouton, calcium transients were stable from episode to episode and over time, with minimal rundown (data not shown). However, different boutons showed a large variation in both peak calcium transient amplitude and transient decay time constant (Fig. 1d, g), indicating heterogeneity of calcium influx and clearance rate among individual PF boutons, as has already been shown by previous studies [28,29]. Variation was also seen in burst peak and summation ratio (defined as the ratio of the burst peak to single peak; Fig. 1j, m). To determine if this variance was also observed among boutons on the same granule cell axon, we next compared calcium transients on a single axon. Measuring transients from boutons of a single axon is a conservative approach, which minimizes differences due factors such as dye-loading variation, differences in axon depth, and axon-to-axon variation in action potential waveform, thereby providing a better measure of true bouton-to-bouton variation. Calcium transients were measured at three neighboring boutons sequentially (Fig. 1a), and the maximum percentage difference in calcium transient peak and decay constant was plotted (Fig. 1e, h). A large variation was found even when boutons of a single axon were compared, with up to almost twofold differences in both calcium transient peak and decay time constant. Variation was also observed in the burst peak and summation ratio in boutons from a single axon (Fig. 1k, n).

Next, we investigated whether differences in bouton volume can account for the observed heterogeneity. Assuming that calcium influx and efflux takes place only through calcium channels and transporters present on the bouton membrane, and that these channels and transporters are present in axonal membranes at a constant density, then it is expected that smaller boutons with a higher surface area to volume ratio will exhibit larger calcium transients and higher calcium clearance rates. To test this hypothesis, we selected every axon where the biggest bouton is at least 60% larger in volume than the smallest bouton, and then compared the calcium influx and decay time constant between the biggest and smallest

boutons. By this selection criteria, on a Z-projected image, the biggest boutons average 1.46±0.09 μm^2 in area, and the smallest boutons average 0.58±0.03 μm^2 in area (Fig. 1c). Surprisingly, the biggest and smallest boutons are not significantly different in calcium transient single peak (Fig. 1f), burst peak (Fig. 1l), and summation ratio (Fig.1o), and only modestly (but significantly) different in decay time constant (Fig. 1i). Essentially, the same results were obtained when the experiments were performed in the presence of synaptic blockade with 10 μM SR95531, a $GABA_A$ receptor antagonist; 50 μM D-APV, an NMDA receptor antagonist; and 10 μM NBQX-Na_2, an AMPA receptor antagonist (Supplemental Fig. 1). These results suggest that mechanisms in boutons compensate for differences in surface area to volume ratio, and that bouton volume is not a significant factor in the heterogeneity of calcium dynamics [28,29].

In addition to heterogeneity in the calcium influx and clearance of individual boutons, we also observed heterogeneity in the mode of calcium clearance after influx caused by a burst of action potentials. Specifically, we noticed that, while the burst peak in the majority of boutons decayed with a single-exponential function similar to the decay seen in single peaks, in a minority of boutons (42% of the total population), the burst peak decayed with a double-exponential function (Fig. 2b). Double-exponential decay occurred only with burst peaks; virtually all single peaks showed single-exponential decay (only 4% of single peaks showed double-exponential decay). We classified boutons as exhibiting double-exponential decay if a double-exponential function curve fit resulted in a correlation coefficient (χ^2) that is at least 10% higher than the correlation coefficient from a single-exponential curve fit. In order to investigate the parameters that predisposed boutons to double-exponential decay, we again measured calcium transients from three neighboring boutons on a single axon in response to both single and burst action potentials (Figs. 1b and 2a), and then segregated boutons on each axon according to four parameters: single peak amplitude, single peak decay constant, burst peak amplitude, and bouton size. We then determined the proportion of double-exponential decay to single-exponential decay in each group. To determine whether calcium clearance mode is correlated to single peak amplitude, single peak decay constant, and burst peak amplitude, we selected axons where the largest response was at least 10% higher than the smallest response, and then determined the frequency of double-exponential decay in the two groups of boutons. To determine whether calcium clearance mode is correlated to bouton volume, we also selected axons where the biggest bouton was at least 60% larger in volume than the smallest bouton and again determined the frequency of double-exponential decay among the two groups. The frequencies of double-exponential decay were similar between boutons showing the largest and smallest single peak amplitude (Fig. 2c), while boutons with a larger single peak decay constant had a higher proportion of double-exponential decay boutons (Fig. 2e). With boutons under synaptic blockade, this relationship was reversed. The frequency of double-exponential decay boutons was higher in boutons with the largest single peak amplitudes (Supplemental Fig. 2f), while the frequencies of double-exponential decay boutons were similar between boutons showing the largest and smallest single peak decay constant (Supplemental Fig. 2e). However, both with and without synaptic blockade, boutons with the highest burst peaks and biggest bouton volumes showed higher frequencies of double-exponential decay boutons (Fig. 2d, f, Supplemental Fig. 2d, f). These results suggests that high calcium influx caused by burst firing can activate an additional calcium clearance mechanism in a subpopulation of large granule cell boutons, which results in a biphasic double-exponential calcium clearance mode.

Previous studies have come to conflicting conclusions about the functional equivalence of AA-PC and PF-PC synapses, a question of considerable importance in cerebellar learning models. To address this question, we examined boutons near the T-junction of the granule cell axon (Fig. 3a), where an AA bifurcates to form PFs, thus allowing us to measure the

calcium dynamics of AA and PF boutons located on the same axon simultaneously. Granule cell axons were stimulated with a single pulse followed 500 ms later by a burst of four pulses at 100 Hz (Fig. 3b), and calcium imaging was performed sequentially on AA and PF boutons in random order (Fig. 3a). We determined the average area of the AA and PF boutons from a Z-projected image of the high-resolution image stack obtained after every experiment and found that AA and PF boutons are similar in area (Fig. 3c). The calcium transients of AA and PF boutons also showed similar single peak amplitude (Fig. 3d), decay time constant (Fig. 3e), burst peak amplitude (Fig. 3f), and summation ratio (Fig. 3g); and similar results were obtained under synaptic blockade (Supplemental Fig. 3). Therefore, boutons on the AA and PF show similar properties in their action potential-evoked calcium response, suggesting a postsynaptic origin for the differences in their synaptic transmission and plasticity properties.

Next, we wanted to determine if boutons located in different layers of the molecular layer exhibit differences in their calcium dynamics. We compared boutons located in the inner one-third of the molecular layer with boutons located in the other third of the molecular layer. Experiments on inner and outer molecular layer boutons were performed in an interleaved manner. Again, we evoked action potential induced calcium transients in the boutons with a stimulation consisting of a single pulse followed by a burst of pulses (Fig. 4c, d) and measured the calcium transients at three neighboring boutons sequentially (Fig. 4a, b). Consistent with previous anatomical studies, we found that boutons in the inner molecular layer were slightly bigger in size compared to boutons in the outer molecular layer (Fig. 4g). Boutons in the inner and outer molecular layer were similar in single peak amplitude (Fig. 4e), burst peak amplitude (Fig. 4f), and summation ratio (Fig. 4i). Surprisingly, however, boutons in the inner molecular layer showed a smaller decay time constant than boutons in the outer molecular layer (Fig. 4h), suggesting that calcium clearance rate is higher in the inner molecular layer boutons. Again, similar results were obtained in the presence of synaptic blockade (Supplemental Fig. 4). The finding that calcium clearance rate is higher in the inner molecular layer boutons is unexpected because inner boutons are slightly larger than outer boutons (Fig. 4h), which would imply a smaller surface area to volume ratio and thus a lower clearance rate. Furthermore, this result cannot be explained by differential loading of calcium-binding dyes into the axons because the mean pixel value of the morphology dye in the inner and outer boutons are similar (Fig. 4j), suggesting equal concentrations of dye in inner and outer boutons. Hence, our data suggests that boutons in the inner molecular layer clear calcium more efficiently than those in the outer layer, which may affect synaptic properties such as short-term plasticity.

Discussion

We have measured calcium dynamics in single presynaptic boutons in PFs of the cerebellum and found that individual boutons show a large variation in peak calcium influx and calcium clearance rate. Peak calcium influx is not correlated to bouton volume, while calcium clearance is slightly slower in boutons of larger volume. Larger boutons with lower calcium clearance rates during single action potential stimulation also tend to exhibit double-exponential calcium clearance curves during burst action potential stimulation. We also could not find any significant difference in the calcium clearance dynamics of PF and AA boutons. Specifically, the calcium transients of AA and PF boutons showed similar single peak amplitude, decay time constant, burst peak amplitude, and summation ratio. Lastly, we found that boutons located in the inner molecular layer have a higher calcium clearance rate compared to boutons in the outer molecular layer, despite boutons in the inner molecular layer having a larger volume. With the exception of a portion of the double-exponential calcium clearance rate data, we obtained largely similar results in boutons under complete synaptic blockade, suggesting that these properties are intrinsic to the granule cell boutons

and are independent of network effects. A caveat to the above finding is that only AA and PF boutons within 500 μm of the T-junction were sampled.

Our findings agree with a previous study which found substantial heterogeneity in calcium dynamics among PF boutons, even when the boutons are on a single axon [28]. Surprisingly, we found that this heterogeneity is not correlated to the size of the boutons. The single compartment model predicts that, assuming that a constant density of calcium channels and transporters are present in presynaptic membranes, bigger boutons with a lower surface area to volume ratio should have a smaller calcium transient peak and a slower calcium clearance rate compared to smaller boutons. The fact that big and small boutons exhibit similar calcium transient peaks suggest that mechanisms exist that normalize calcium influx in boutons of different sizes, perhaps by altering the density of calcium channels and transporters at individual boutons, or by the presence of the internal calcium stores in a subpopulation of boutons. It is also possible that other factors such as postsynaptic dendritic compartment or heterogeneity among PCs may be responsible for the variation in calcium dynamics. Heterogeneity in presynaptic calcium dynamics is likely to contribute to heterogeneity in synaptic transmission and may affect both short and long-term plasticity at this synapse.

In addition, we observed that in response to bursts of action potentials, calcium transients sometimes exhibit a double-exponential decay. A number of previous studies have documented that large or prolonged calcium transients, particularly those evoked by trains of action potentials, show biphasic decay curves, whereas smaller calcium transients evoked by single action potentials exhibit mono-exponential decay. While this phenomenon has not been extensively characterized, a number of mechanisms have been suggested, including buffer non-linearities [32], calcium dependent regulation of calcium extrusion [33], intrinsic non-linearities in calcium transporters, and diffusion of calcium into adjacent compartments [34]. Although the mechanism of this phenomenon is unclear, given its prevalence in a number of different preparations and synapses, it is likely that the biphasic decay constitutes a widespread and fundamental physiological mechanism for calcium clearance that is activated by high calcium influx.

The roles of the AA and PF synapses in cerebellar function have been a topic of much debate and controversy. While some studies have suggested that AA inputs provide a stronger synaptic drive to PCs compared to PF inputs, other studies have found no differences between both types of synapses. In this study, we found that AA and PF boutons do not differ significantly in both single and burst action potential-evoked calcium influx and clearance. This similarity in calcium dynamics indicate that there is no difference in the presynaptic efficacy of AA and PF boutons, broadly in agreement with previous studies studying unitary transmission at AA-PC and PF-PC synapses [15,16]. While the functional equivalence of AA and PF synapses may seem to be incompatible with the patchy activation of PCs by physiological stimuli found in many in vivo studies, a recent study has found that when inhibition is blocked, a patch of granule cells activated by physiological tactile stimuli now activates a row of PCs, a result which suggest that AA and PF synapses possess similar synaptic strengths and that patchy activation of PCs arises not because of stronger AA inputs but because of feedforward inhibition [35].

Finally, we found that PF boutons located in the inner molecular layer have a higher calcium clearance rate than boutons located in the outer molecular layer, which is surprising because the single compartment model predicts that the larger boutons of the inner molecular layer should have a lower calcium clearance rate. We believe that our findings are the first demonstration to date of a functional difference between boutons located in different regions of the cerebellar molecular layer. These findings were preceded by several studies showing

numerous anatomical differences between PFs in the inner and outer molecular layers. Compared to the PFs in the outer molecular layer, PFs in the inner molecular layer are shorter, thicker, and have larger boutons [17,20]. PFs in the different regions arise from different granule cells, synapse on different interneurons, and different regions of the PC dendritic tree. Our findings suggest that these anatomical differences are reflected in a functional difference between boutons in the different layers. This layer-specific functional difference may be a mechanism for differential processing of information arising from different inputs into the cerebellum.

Conclusion

Classical theories of cerebellar learning assume that all PF-PC synapses are homogeneous in properties. Our findings indicate that these theoretical models have to be altered to take into account heterogeneity in the properties of these synapses. Heterogeneity in synaptic properties may serve as a physiological basis for the encoding of different forms of learning in the same circuitry. For example, the cerebellum is involved in several forms of motor learning. Some learning paradigms, such as eyeblink conditioning, are accompanied by long-term depression and synapse elimination in the PF-PC synapse, while others, such as acrobatic training, are accompanied by long-term potentiation and synapse formation. In order for the memory traces of different forms of learning to not interfere with each other, it is possible that they operate on different subsets of PF-PC synapses. Differences in calcium dynamics among boutons can contribute to heterogeneity in synaptic efficacy and plasticity, which may serve to increase the computational capacity of the brain.

Supplementary Material

Refer to Web version on PubMed Central for supplementary material.

Acknowledgments

We thank members of the Linden laboratory for helpful comments and discussion and Devorah VanNess for providing technical assistance. This work was supported by NIH MH51106 and the Develbiss Foundation.

References

1. Napper RM, Harvey RJ. Number of parallel fiber synapses on an individual Purkinje cell in the cerebellum of the rat. J Comp Neurol. 1988; 274(2):168–177. [PubMed: 3209740]
2. Palay, SL.; Chan-Palay, V. Cerebellar cortex: cytology and organization. Springer-Verlag, Berlin; 1974.
3. Braitenberg V, Atwood RP. Morphological observations on the cerebellar cortex. J Comp Neurol. 1958; 109(1):1–33. [PubMed: 13563670]
4. Eccles, JC.; Ito, M.; Szentagothai, J. The cerebellum as a neuronal machine. Springer; Berlin: 1967.
5. Eccles JC, Llinas R, Sasaki K. Parallel fibre stimulation and the responses induced thereby in the Purkinje cells of the cerebellum. Exp Brain Res. 1966; 1(1):17–39. [PubMed: 5910940]
6. Coutinho V, Mutoh H, Knopfel T. Functional topology of the mossy fibre-granule cell—Purkinje cell system revealed by imaging of intrinsic fluorescence in mouse cerebellum. Eur J NeuroSci. 2004; 20(3):740–748. [PubMed: 15255984]
7. Eccles JC, Sabah NH, Schmidt RF, Taborikova H. Integration by Purkyne cells of mossy and climbing fiber inputs from cutaneous mechanoreceptors. Exp Brain Res. 1972; 15(5):498–520. [PubMed: 4634429]
8. Kolb FP, Arnold G, Lerch R, Straka H, Buttner-Ennever J. Spatial distribution of field potential profiles in the cat cerebellar cortex evoked by peripheral and central inputs. Neuroscience. 1997; 81(4):1155–1181. [PubMed: 9330375]

9. Bower JM, Woolston DC. Congruence of spatial organization of tactile projections to granule cell and Purkinje cell layers of cerebellar hemispheres of the albino rat: vertical organization of cerebellar cortex. J Neurophysiol. 1983; 49(3):745–766. [PubMed: 6300353]
10. Cohen D, Yarom Y. Patches of synchronized activity in the cerebellar cortex evoked by mossy-fiber stimulation: questioning the role of parallel fibers. Proc Natl Acad Sci U S A. 1998; 95(25): 15032–15036. [PubMed: 9844010]
11. Gao W, Chen G, Reinert KC, Ebner TJ. Cerebellar cortical molecular layer inhibition is organized in parasagittal zones. J Neurosci. 2006; 26(32):8377–8387. [PubMed: 16899733]
12. Bower JM. The organization of cerebellar cortical circuitry revisited: implications for function. Ann N Y Acad Sci. 2002; 978:135–155. [PubMed: 12582048]
13. Sims RE, Hartell NA. Differences in transmission properties and susceptibility to long-term depression reveal functional specialization of ascending axon and parallel fiber synapses to Purkinje cells. J Neurosci. 2005; 25(12):3246–3257. [PubMed: 15788782]
14. Sims RE, Hartell NA. Differential susceptibility to synaptic plasticity reveals a functional specialization of ascending axon and parallel fiber synapses to cerebellar Purkinje cells. J Neurosci. 2006; 26(19):5153–5159. [PubMed: 16687506]
15. Isope P, Barbour B. Properties of unitary granule cell→ Purkinje cell synapses in adult rat cerebellar slices. J Neurosci. 2002; 22(22):9668–9678. [PubMed: 12427822]
16. Walter JT, Dizon MJ, Khodakhah K. The functional equivalence of ascending and parallel fiber inputs in cerebellar computation. J Neurosci. 2009; 29(26):8462–8473. [PubMed: 19571137]
17. Pichitpornchai C, Rawson JA, Rees S. Morphology of parallel fibres in the cerebellar cortex of the rat: an experimental light and electron microscopic study with biocytin. J Comp Neurol. 1994; 342(2):206–220. [PubMed: 8201032]
18. Gundappa-Sulur G, De Schutter E, Bower JM. Ascending granule cell axon: an important component of cerebellar cortical circuitry. J Comp Neurol. 1999; 408(4):580–596. [PubMed: 10340507]
19. Lu H, Esquivel AV, Bower JM. 3D electron microscopic reconstruction of segments of rat cerebellar Purkinje cell dendrites receiving ascending and parallel fiber granule cell synaptic inputs. J Comp Neurol. 2009; 514(6):583–594. [PubMed: 19363797]
20. Sultan F. Exploring a critical parameter of timing in the mouse cerebellar microcircuitry: the parallel fiber diameter. Neurosci Lett. 2000; 280(1):41–44. [PubMed: 10696807]
21. Chadderton P, Margrie TW, Hausser M. Integration of quanta in cerebellar granule cells during sensory processing. Nature. 2004; 428(6985):856–860. [PubMed: 15103377]
22. D'Angelo E, De Zeeuw CI. Timing and plasticity in the cerebellum: focus on the granular layer. Trends Neurosci. 2009; 32(1):30–40. [PubMed: 18977038]
23. Jorntell H, Ekerot CF. Properties of somatosensory synaptic integration in cerebellar granule cells in vivo. J Neurosci. 2006; 26(45):11786–11797. [PubMed: 17093099]
24. Rancz EA, Ishikawa T, Duguid I, Chadderton P, Mahon S, Hausser M. High-fidelity transmission of sensory information by single cerebellar mossy fibre boutons. Nature. 2007; 450(7173):1245–1248. [PubMed: 18097412]
25. Helmchen F, Borst JG, Sakmann B. Calcium dynamics associated with a single action potential in a CNS presynaptic terminal. Biophys J. 1997; 72(3):1458–1471. [PubMed: 9138591]
26. Regehr WG, Atluri PP. Calcium transients in cerebellar granule cell presynaptic terminals. Biophys J. 1995; 68(5):2156–2170. [PubMed: 7612860]
27. Pelkey KA, Topolnik L, Lacaille JC, McBain CJ. Compartmentalized Ca(2+) channel regulation at divergent mossy-fiber release sites underlies target cell-dependent plasticity. Neuron. 2006; 52(3): 497–510. [PubMed: 17088215]
28. Brenowitz SD, Regehr WG. Reliability and heterogeneity of calcium signaling at single presynaptic boutons of cerebellar granule cells. J Neurosci. 2007; 27(30):7888–7898. [PubMed: 17652580]
29. Zhang W, Linden DJ. Neuromodulation at single presynaptic boutons of cerebellar parallel fibers is determined by bouton size and basal action potential-evoked Ca transient amplitude. J Neurosci. 2009; 29:15586–15594. [PubMed: 20007482]

30. Beierlein M, Gee KR, Martin VV, Regehr WG. Presynaptic calcium measurements at physiological temperatures using a new class of dextran-conjugated indicators. J Neurophysiol. 2004; 92(1):591–599. [PubMed: 15212445]

31. Kreitzer AC, Gee KR, Archer EA, Regehr WG. Monitoring presynaptic calcium dynamics in projection fibers by in vivo loading of a novel calcium indicator. Neuron. 2000; 27(1):25–32. [PubMed: 10939328]

32. Tank DW, Regehr WG, Delaney KR. A quantitative analysis of presynaptic calcium dynamics that contribute to short-term enhancement. J Neurosci. 1995; 15(12):7940–7952. [PubMed: 8613732]

33. Scheuss V, Yasuda R, Sobczyk A, Svoboda K. Nonlinear [Ca2+] signaling in dendrites and spines caused by activity-dependent depression of Ca2+ extrusion. J Neurosci. 2006; 26(31):8183–8194. [PubMed: 16885232]

34. Koester HJ, Sakmann B. Calcium dynamics associated with action potentials in single nerve terminals of pyramidal cells in layer 2/3 of the young rat neocortex. J Physiol. 2000; 529(Pt 3): 625–646. [PubMed: 11118494]

35. Santamaria F, Tripp PG, Bower JM. Feedforward inhibition controls the spread of granule cell-induced Purkinje cell activity in the cerebellar cortex. J Neurophysiol. 2007; 97(1):248–263. [PubMed: 17050824]

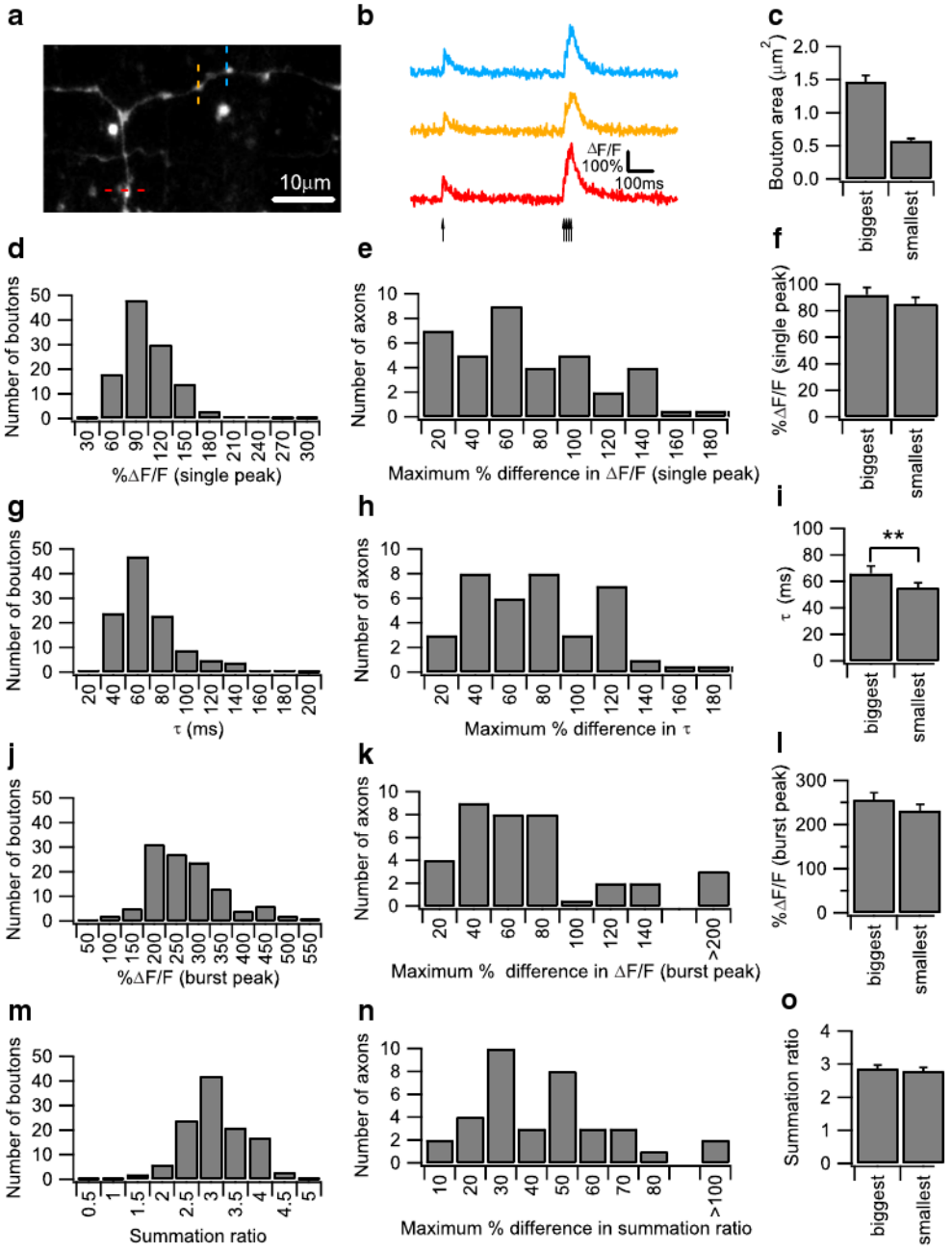

Fig. 1.

Heterogeneity of action potential (AP)-evoked Ca^{2+} transients in granule cell axonal boutons. **a** A Z-projection confocal stack image showing a dye-loaded parallel fiber (PF). Individual boutons appear as bead-like varicosities along axons. Ca^{2+} imaging was performed sequentially on three individual boutons located on the ascending axon or the PF as indicated by the *red, yellow*, and *blue dotted lines*. This confocal stack image was projected by summing pixel intensities. **b** Representative AP-evoked Ca^{2+} transients measured from three neighboring boutons on the same PF shown in (**a**) were plotted as $\Delta F/F$ over time. Ca^{2+} transients were evoked by a protocol consisting of a single AP followed 500 ms later by a burst of four pulses at 100 Hz. The arrows indicate the onset of the individual AP. The averaged traces from ten trials are shown. **c** *Bar graph* showing average bouton

areas of the biggest and smallest boutons on a single PF axon, measured from 34 axons. Bouton areas were determined from the Z-projection of confocal images of the dye-filled bouton obtained after calcium imaging. Histograms of the single AP-evoked Ca^{2+} peak amplitude (**d**) and decay time constant (**g**), as well as the burst AP-evoked peak amplitude (**j**) and summation ratio (**m**) from 115 granule cell boutons, are presented. The summation ratio was calculated as the peak Ca^{2+} transient evoked by the burst AP divided by the peak Ca^{2+} transient evoked by the single AP. Histograms of the maximum percentage difference in single AP-evoked Ca^{2+} response amplitude (**e**) and decay time constant (**h**), as well as the burst AP-evoked Ca^{2+} response amplitude (**k**) and summation ratio (**n**) from three boutons measured on the same axon from 36 axons, are presented. Comparison of various parameters between the biggest and smallest boutons on the same axon. Axons were only included if the biggest bouton was at least 60% larger in volume compared with the smallest bouton, and 34 axons were compared in total. *Bar graphs* showing the single AP-evoked Ca^{2+} response amplitude (**f**) and decay time constant (**i**), as well as the burst AP-evoked Ca^{2+} response amplitude (**l**) and summation ratio (**o**), are shown. *Error bars* indicate the SEM in this and all subsequent figures

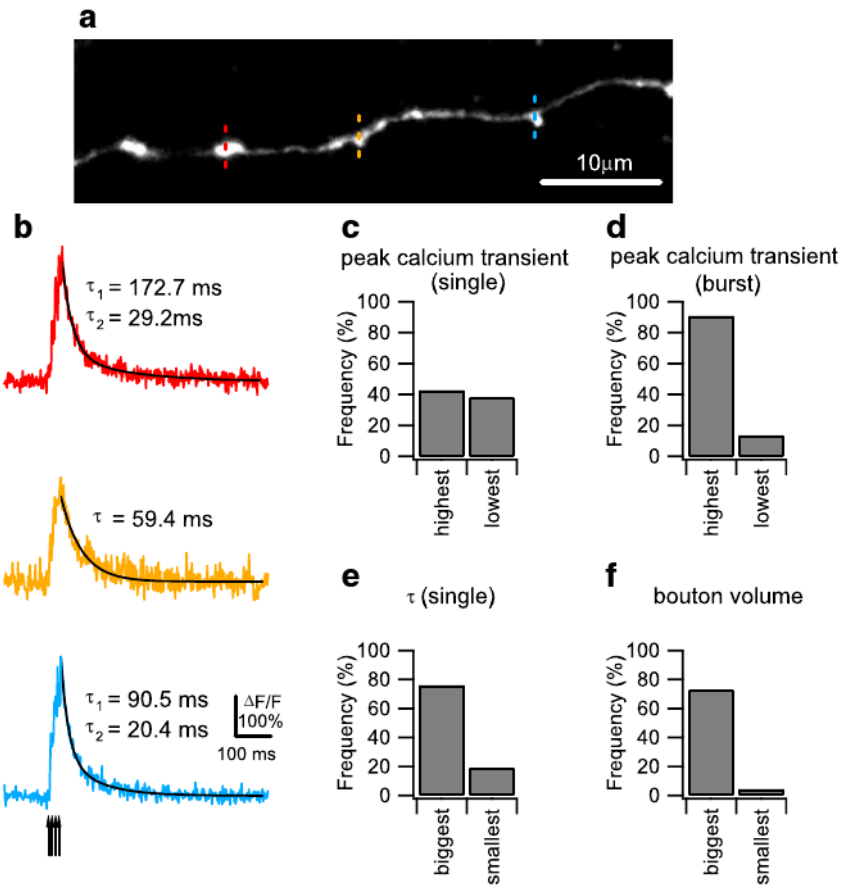

Fig. 2.

Double- and single-exponential decay time course of action potential (AP)-evoked Ca^{2+} transients in granule cell axonal boutons. **a** A Z-projection confocal stack image showing a representative dye-loaded parallel fiber (PF). Ca^{2+} imaging was performed sequentially on three individual boutons indicated by the *red, yellow*, and *blue dotted lines*. The confocal stack image was projected by summing pixel intensities. **b** Burst (four pulses at 100 Hz) AP-evoked Ca^{2+} transients measured sequentially from three neighboring boutons on the same PF shown in (**a**). The average traces from five trials are shown. Ca^{2+} responses were well fit by single-exponential decay curve (*yellow*) or double-exponential curves (*red* and *blue*), shown as superimposed *black lines*. The *arrow* indicates the onset of the individual AP during the burst stimulation. Comparison of the frequency of occurrence of double-exponential decay mode of calcium clearance in different groups of granule cell boutons. To divide boutons into two groups based on their single AP-evoked Ca^{2+} response amplitude and decay time constant and burst AP-evoked Ca^{2+} response amplitude, we included axons only if the difference between the largest and smallest response was at least 10% of the smallest response. To divide boutons based on volume, we only included axons where the biggest bouton was at least 60% larger in volume compared with the smallest bouton. *Bar graphs* showing the percentage frequency of boutons exhibiting double-exponential decay time course in groups of boutons divided by single AP-evoked Ca^{2+} response amplitude (**c**; 21 axons), burst AP-evoked Ca^{2+} response amplitude (**d**; 22 axons), single AP-evoked Ca^{2+} response decay time constant (**e**; 21 axons), and bouton volume (**f**; 22 axons) are presented

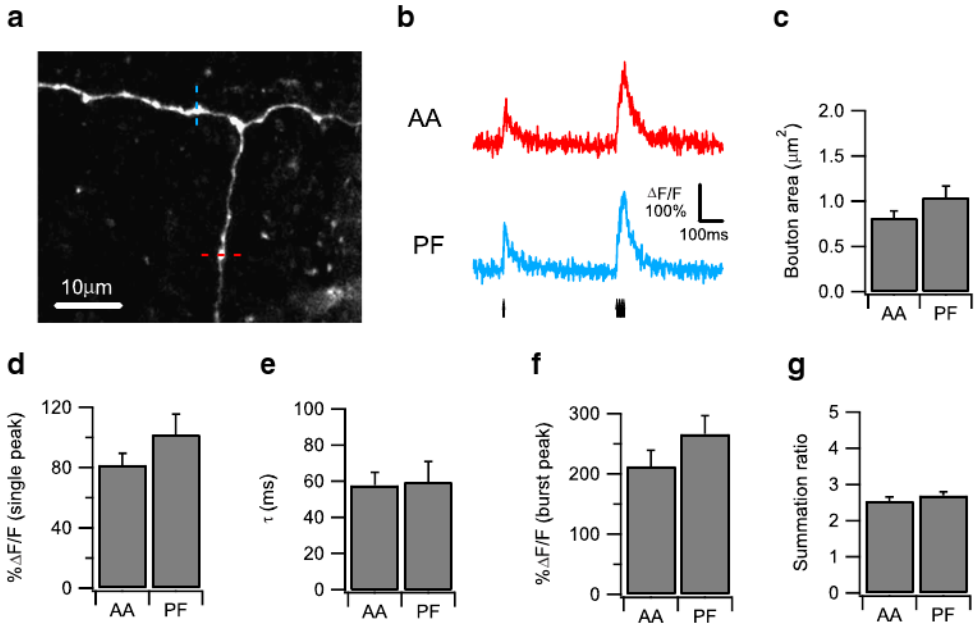

Fig. 3.

Boutons on the ascending axon (AA) and the parallel fiber (PF) show similar properties in action potential (AP)-evoked Ca^{2+} response. **a** A Z-projection confocal stack image showing a representative dye-loaded granule cell axon with PF bifurcated from AA. AP-evoked Ca^{2+} responses were measured sequentially at the individual boutons on the AA (indicated by *red dotted line*) and PF (indicated by *blue dotted line*). **b** Representative AP-evoked Ca^{2+} transients measured from an AA bouton (*red*) and a PF bouton (*blue*) on the same granule cell axon shown in (**a**) plotted as $\Delta F/F$ over time. Ca^{2+} transients were evoked by a protocol consisting of a single AP followed 500 ms later by a burst of four pulses at 100 Hz. The *arrows* indicate the onset of the individual AP. The averaged traces from ten trials are shown. *Bar graphs* comparing the bouton area (**c**), the single AP-evoked Ca^{2+} response amplitude (**d**), the single AP-evoked Ca^{2+} response decay time constant (**e**), the burst AP-evoked Ca^{2+} response amplitude (**f**), and the Ca^{2+} response summation ratio (**g**) between an AA bouton and a PF bouton on the same axon are shown, measured from 16 pairs of boutons on ten axons

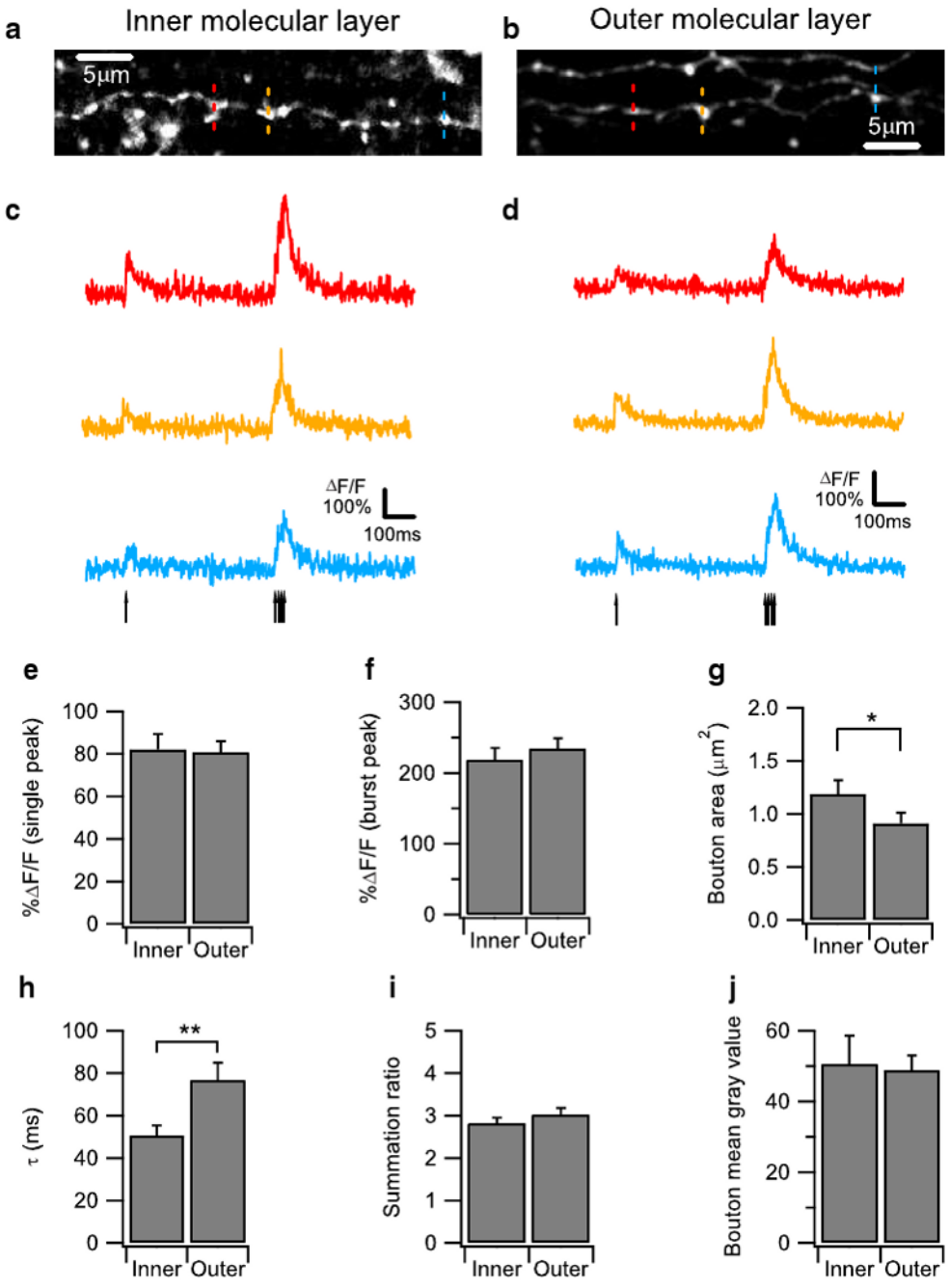

Fig. 4.

Parallel fiber (PF) boutons located in the outer molecular layer show slower action potential (AP)-evoked Ca^{2+} response decay kinetics than those in inner molecular layer. **a**, **b** Z-projection confocal stack images showing a dye-loaded PF located in inner molecular layer (**a**) and outer molecular layer (**b**), respectively. Ca^{2+} imaging was performed sequentially on three individual boutons located on the PFs as indicated by the *red, yellow*, and *blue dotted lines*. This confocal stack image was projected by summing pixel intensities. **c, d** Representative AP-evoked Ca^{2+} transients measured from three neighboring boutons on the same PFs in the inner molecular layer (**a**) and outer molecular layer (**b**) were plotted as $\Delta F/F$

over time. Ca^{2+} transients were evoked by a protocol consisting of a single AP followed 500 ms later by a burst of four APs at 100 Hz The *arrows* indicate the onset of the individual AP. The averaged traces from ten trials are shown. *Bar graphs* comparing (**e**), (**f**), (**h**), and (**i**) are bar graphs showing the single AP-evoked Ca^{2+} response amplitude (**e**), the burst AP-evoked Ca^{2+} response amplitude (**f**), single AP-evoked Ca^{2+} response decay time constant (**h**), and the Ca^{2+} response summation ratio (**i**) between PF boutons located in the inner and the outer molecular layers are shown. PF boutons located in outer molecular layer show a larger single AP-evoked Ca^{2+} response decay time constant than those in inner molecular layer (**h**), indicating slower decay kinetics. **g** *Bar graph* comparing the bouton areas of PF boutons located in the inner and outer molecular layers. **j** *Bar graph* showing the bouton's mean gray value comparing the PF boutons located in the inner molecular layer and the outer molecular layer. 21 boutons from seven PFs were quantified for each group